Evaluation of wave energy converter arrays within a sheltered bay

Emiliano N. Gorr-Pozzi, Héctor García-Nava, Melissa G. Jaramillo-Torres, Marco J. Larrañaga-Fu, Francisco J. Ocampo-Torres

Abstract—**The extraction of energy from renewable sources is currently envisioned as a possible solution to the global energy crisis. Ocean waves are one of the most promising sources of energy because their high energy density per unit area and because energy naturally flows to the coast where it can be harvested more easily. However, most Wave Energy Converters (WECs) are designed to work in relatively high seas. This limits their performance in tropical regions, typically dominated by gentle swell. The present study analyzes and compares the performance of two types of WECs within a sheltered bay in the subtropical zone. To analyze the wave climate in the area a ten-year hindcast is performed. Then, the extraction of energy with Pelamis and Oyster2 is simulated based on its power matrix. Finally, different array configurations are examined. In accordance with the results, the studied area has several sites suitable for wave energy extraction. The area has a moderate available wave power with a clear seasonality and a large spatial variability caused by the sheltering effect of Todos Santos Island. Both analyzed devices work better in the southern region; however, Pelamis is more effective than Oyster2 on extracting the available wave power. All the different WEC array configurations examined induced changes near-field and nearshore.**

Keywords— **Numerical wave modeling, renewable energy sources, wave energy extraction, wave farm arrays.**

Paper ID number: #1443. Conference track: Wave resource characterization. This work was supported by the Mexican Center for Innovation in Oceanic Energy (CEMIE-Oceano).

E. N. Gorr-Pozzi and H. García-Nava are with Oceanological Research Institute (IIO) of the Autonomous University of Baja California (UABC), Ensenada, Baja California, 22860 México (e-mail: emigorr@uabc.edu.mx, hector.gnava@uabc.edu.mx).

M. G. Jaramillo-Torres, M. J. Larrañaga-Fu and F. J. Ocampo-Torres are with the Department of Physical Oceanography, CICESE, Carretera Ensenada-Tijuana 3918, Ensenada, Baja California, 22860 México (e-mail: jaramillo@cicese.edu.mx, mlarranaga@cicese.edu.mx, ocampo@cicese.mx).

I. Introduction

NOWADAYS there is a growing trend in the planetary energy demand. Although the development of new technologies has significantly reduced the greenhouse gas consumption, the constant increase of the population and the rise of certain activities create an evident panorama in the search and use of new ways of cleaner energy [1]. Renewable energy has become a credible alternative to fossil fuels for meeting the increasing energy demand of industrialized societies [2]. Proof of this is the enactment of the Mexican Energy Transition Law that provides a framework for clean energy, energy efficiency and greenhouse gas emission reductions. This Law establishes that by 2024, 35% of electricity generation must come from clean energies [3].

The best known renewable energy sources are hydroelectric, biomass, wind, geothermal and solar. However, there is a potential in the energy extracted from the ocean that is still missing to exploit in a greater capacity. The Pacific Coast of North America has one of the most important marine renewable energy resources in the world in terms of waves [4]. In particular, wave energy has the advantage of being predictable and that it naturally flows to zones where it can be used.

The wave power potential has been estimated to be between 1 TW and 10 TW of power, which is of the same order of magnitude as world electrical energy consumption [5]. Large values of wave power (larger than 60 kW/m) are located in extra tropical zones in both hemispheres [6]. However, it cannot be harnessed effectively everywhere and it depends on the characteristics of the waves in the zone of interest as well as on the available technology deployed.

Wave Energy Converters (WECs) extract energy directly from the surface motion of ocean waves or from pressure fluctuations below the surface. This technology has been developed to harvest wave energy from shoreline to deep-water areas. Onshore and shallow water systems usually are embedded in the shoreline or moored close to shore. This has the advantage of easier installation and maintenance and would not require long lengths of underwater electrical cables to connect with the power grid or expensive deep-water moorings. However, close to shore systems usually operate under a less powerful wave regime and could be subjected to

 Copyright © European Tidal and Wave Energy Conference 2019

potentially dangerous loads due to wave breaking. Offshore devices typically consist of floating bodies at depths greater than 40 m.

Commonly, to extract wave energy at a commercial scale it is necessary to install arrays of multiple WECs. To understand the possible implications of these systems, composed of tens or hundreds of individual obstacles, at the leeward area of the deployment site and on the nearshore environment, it must be considered to minimize the potential impact on the nearshore wave propagation and circulation patterns [7]. The far-field effects of WEC arrays include a redirection of waves and a reduction in wave height in the lee of the array, referred to as wake of energy reduction. The magnitude and extent of the far-field effects of WEC arrays are a function of the array configuration, its location, and the incident wave conditions.

The main goal of this study is to evaluate the WECs performance in Todos Santos Bay. For this purpose, the spatial and temporal variability of the wave power was determined and the extracting capacity of two WECs was evaluated. Different array configurations were then tested and their far-field effects evaluated.

II. METHODOLOGY

The performance of two different technologies of WECs was evaluated at Todos Santos Bay, Baja California, Mexico based on numerical simulations.

Numerical simulations are used to determine wave characteristics and to evaluate wave energy availability. The sea-state was characterized by the significant wave height (H_s) and the peak wave period (T_p) to quantify the amount of wave energy that can be extracted with each analyzed WEC type. Finally, the effects of the different WEC arrays on the nearshore area were determined.

A. Field site

Todos Santos Bay (BTS) is located in the northwestern coast of the Baja California peninsula in Mexico (Fig. 1). It is a semi-sheltered bay partially protected from the South Pacific swell by Todos Santos Islands and delimited by Punta San Miguel in the North and Punta Banda Peninsula to the South. The average wave conditions within the bay are dominated by the incoming long period swell (H_s = 1 m and T_p = 11 s). The swell arriving to the area is bimodal all year round, but dominated by northwesterly swell, originated in the extratropical North Pacific, during winter and by southwesterly swell, originated in the extratropical South Pacific, during summer [8]. The incidence of storms is common in the area between October and April with maximum H_s between 3 and 4 m. Calm wave conditions occur from June to September with a mean H_s around 0.7 m.

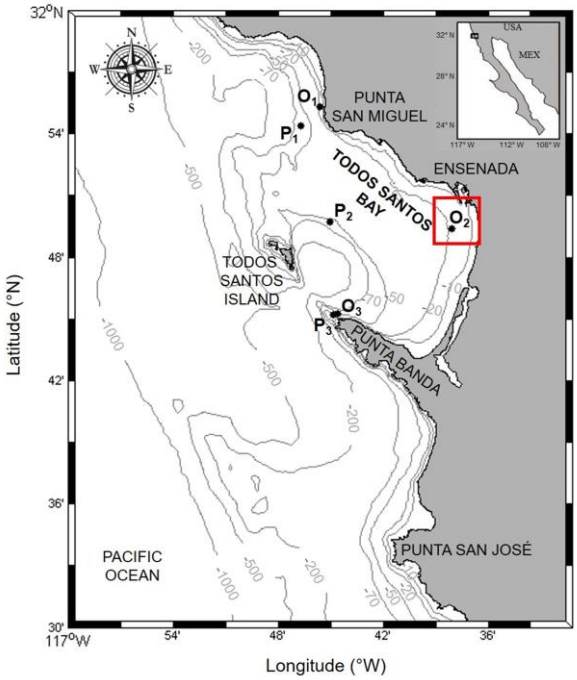

Fig. 1. Location of the study site within the Baja California peninsula. The positions for each evaluated points are indicated. P-points represent the sited areas for Pelamis devices and the O-points for the Oyster2 converter. The red lines show the located of nested grids for the WEC arrays analysis area. The solid lines represent the isobaths and their value is expressed in meters.

B. Model setup

A wave hindcast for the BTS and its surroundings was performed using the third-generation wave model SWAN Cycle IV version 41.01 [9]. The hindcast spans from January 1, 2008 to December 31, 2017 with output data every hour. The model was implemented in an area of 0.5° by 0.5°, from 31°30′ to 32° N and from 117° to 116°30′ W. SWAN model was used in non-stationary two-dimensional mode, the domain was discretized in a regular mesh with a spatial resolution of 0.0025° (approximately 280 m), an equally logarithmic spaced frequency resolution with 41 frequencies, from 0.04 Hz to 0.7 Hz, was used and a directional resolution of 5°.

SWAN model was forced at the boundaries with historic wave fields from the IOWAGA hindcast, which is based on the WAVEWATCH III™ model version 4.04 [10]. Data from IOWAGA used here the PACE subgrid with a 1/6° resolution and forced with global winds from the ECMWF [11].

C. Assessment and variability of potential wave power

Wave power ($\bar{P}$), or wave energy flux, is computed directly from simulated directional spectra as

$$\bar{P} = \rho g \int_0^{\infty} \int_0^{2\pi} c_g E(f,\theta) df d\theta \quad (1)$$

where, ρ is the density of water, g is the gravitational acceleration, c_g is the group velocity, and $E(f,\theta)$ is the two-dimensional variance density spectrum, i.e. the directional spectra.

The seasonal and the year to year variability are characterized with the Mean Annual Variability (MAV), and the Inter-Annual Variability (IAV), computed as [12]

$$MAV = \overline{\left(\frac{\sigma_j}{\bar{\sigma}_j}\right)}, \quad (2)$$

$$IAV = \left(\frac{\sigma_{\bar{X}j}}{\bar{X}}\right), \quad (3)$$

where σ is the standard deviation, $\bar{x}$ is the mean value, the subindex j refer to yearly values and the over bar denotes average.

Wave power is characterized by its mean value and the seasonal patterns are described by averaging the wave power for winter (January to March) and summer (July to September).

D. Quantification of harvestable wave energy

Two relevant worldwide WECs are evaluated in this work, Pelamis [13] and Oyster2 [14]. Pelamis is an attenuator-type device that operates more efficiently in depths between 50 m and 70 m. In contrast, Oyster2 is a bottom-fixed oscillating flap device designed to be harnessed in the nearshore region, usually between 10 m and 20 m depth.

The harvestable wave power *PE* was computed as [15]

$$PE = \sum\sum HR(H_s, T_p) \cdot PWEC(H_s, T_p) \quad (4)$$

where, *HR* is the availability matrix in terms of the occurrence of each sea state and $PWEC$ is the power matrix of the WEC. For the ease of comparison the average *PE* was normalized with the width of each device considered.

The solely analysis of the wave power availability for a certain place can mislead the identification of the most appropriate location for extracting the wave energy [16]. A bivariate distribution represents the probability of occurrence of a particular sea state expressed as a percentage. Diagrams for the bivariate distributions, defined with H_s and the energy period (T_e), were computed to complement the estimations of wave power for three reference points (Fig. 1) distributed from north to south within BTS (offshore P-points for Pelamis and nearshore O-points for Oyster2 devices, respectively).

E. Representation of WEC arrays in SWAN

The numerical model SNL-SWAN was used to simulate WECs arrays within the BTS. SNL-SWAN [17] is a version of the wave model SWAN that incorporates a WEC module developed to evaluate more accurately the WEC farm effects on wave propagation and to improve the capability of the model to estimate the impact of WECs on the nearshore wave climate.

The WEC module calculates the effective transmission coefficient (k_t^2), associated with a WEC's power performance, based on the WEC characteristics [18]. The (k_t^2) represents the power ratio incident and lee of the obstacle, depending on the frequency, which results in a variable power absorption, calculated as

$$k_t^2(f) = 1 - \frac{P_{absorbed}}{P_{incident}} = 1 - RCW(f) \quad (5)$$

where RCW is the Relative Capture Width, a non-dimensionalized power ratio defining the WEC's power performance that is supplied by the user. It represents the ratio between the power absorbed by the WEC ($P_{absorbed}$), which depend on the performance and dimensions of the converter, and the incident power of the wave ($P_{incident}$). Fig. 2 shows the RCW curve used to simulate Oyster2 WEC in the SWAN numerical model. This curve is sampled independently for each frequency of the simulation, resulting in a frequency-dependent obstacle transmission coefficient.

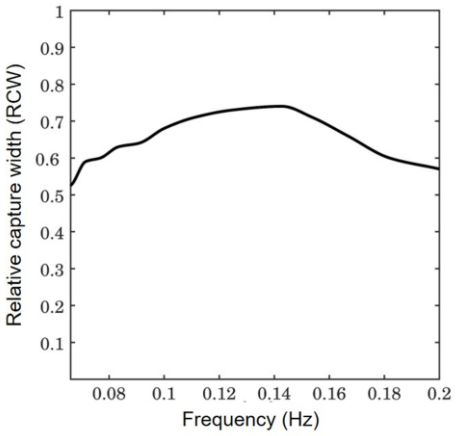

Fig. 2. Oyster2 RCW curve used to calculate K_t applied as a constant value, which shows the portion of energy absorbed for each frequency band in Ref [19].

Because the possible impact of WEC farm facilities is greater nearshore (depth ≤ 35 m), we focus the analysis of the WEC arrays only on the Oyster2 device. A nearshore area within BTS was selected to locate the arrays based on the optimum operating depth range of the WEC. A nested mesh of 26 m resolution was generated, congruent with the width dimension of the selected converter (Fig. 1). The quantification of the changes in the far-field wave conditions as a result of the WEC arrays were carry out for a typically event of the winter season.

For the Oyster2 case, four configurations of WEC arrays were chosen for the analysis of the simulations. The first one consisted in a single obstacle positioned approximately 2500 m from the shoreline. The second consisted of 5 vertically aligned converters with a spacing of 10 times the dimensional width of the flap. This configuration is considered a highly spaced arrangement. It was selected according to previous studies indicating that this type of arrangement affects at a smaller degree the wave parameters, and, therefore, it results to a lower impact on the coast [20]. The third configuration consisted of a number of 10 converters, organized in two rows of 5 devices aligned vertically (2500 m to 2250 m

range from the shoreline) with the same spacing between devices as the second configuration. The last configuration consisted of an array known as staggered, in which the converters were placed in an intercalated manner, adding a total of 25 devices with the same spacing distance of devices between rows and columns (2500 m to 1500 m distance from the coast); this type of arrangement forms a farm of converters that allows a higher rate of energy absorption [20].

III. RESULTS

F. *Wave power availability*

Figure 3 shows the mean wave power for the summer (Fig. 3 (a)) and winter season (Fig. 3 (b)), and the overall wave power (Fig. 3 (c)). As it can be seen the annual mean $\bar{P}$ outside the bay is around 11 kW/m with a maximum of 15 kW/m in the south, influenced by offshore banks and salient formations. Inside the bay the mean wave power is around 8 kW/m, with variations between 5 kW/m in the southern section and 11 kW/m in the northern section. This difference between sections of the bay occurs due to the shadow effect produced by Todos Santos Island. In accordance to those reported by [21] for the Northwest of Baja California, maximum mean values (close to 20 kW/m) are found outside of BTS in geographical headland formations as Punta San Jose during the winter season Fig. 3 (b). Seasonally mean values are 2.5 times higher during winter (15 kW/m, Fig. 3 (b)) than those observed during the summer period (6 kW/m, Fig. 3 (a)); due to the bimodal seasonality of the wave climate that predominate in the area.

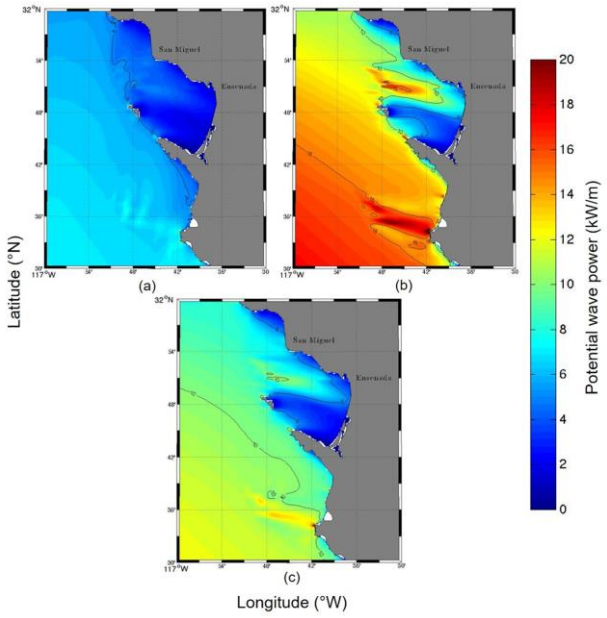

Fig. 3. Distribution of the mean wave power (kWm^{-1}) from January 2008 to December 2017 for (a) summer (July to September) and (b) winter (January to March) seasons, and (c) the annual mean wave power over the full hindcast period.

The MAV and IAV will determine which areas of BTS receive a more regular and constant $\bar{P}$ and which are more variable. Figure 4 shows the mean annual variability (Fig. 4 (a)) and the inter-annual variability (Fig. 4 (b)) of the wave power. In general the IAV is around 0.2 with the most variable areas in the northern section of BTS, and in the external offshore banks and salient formations along the southern coast. The less variable zone is inside the southern section of BTS behind the islands where the IAV is less than 0.15. MAV have a similar pattern as described for IAV with values around 1.0 and maximum of 1.4 which indicate a marked seasonality of wave power.

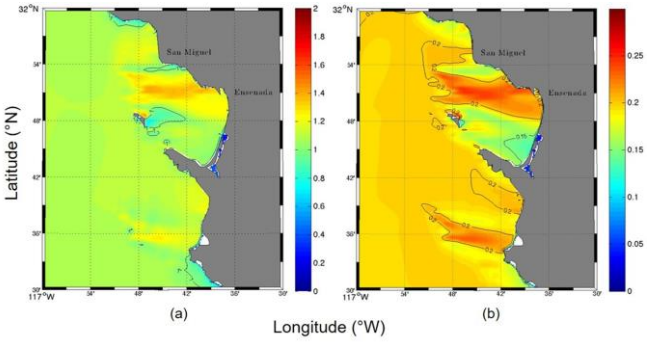

Fig. 4. Mean annual variability (MAV, panel (a) and the inter-annual variability (IAV, panel (b) of the mean wave power, for the period 2008-2017. Both statistical indices are dimensionless.

G. *Harvested wave power*

The mean $\bar{P}$ harvested by Pelamis and Oyter2 devices is shown in Fig. 5 (d) and Fig. 6 (d), respectively. To ease the comparison between both devices, we selected 3 points distributed from North to South in BTS, within the optimum operating depth range associated with each WEC: P_1, P_2, P_3 for Pelamis and O_1, O_2, O_3 for Oyster2.

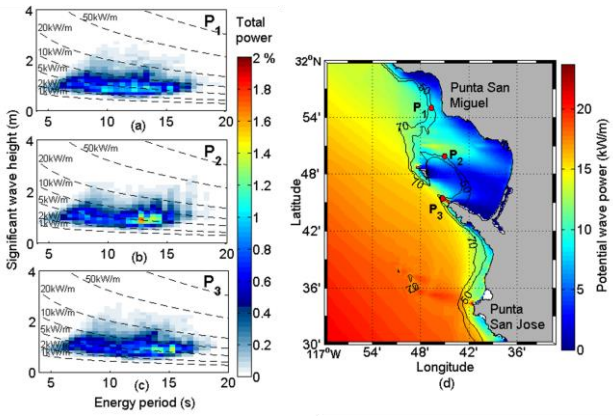

Fig. 5. Annual mean wave energy, harvested by the Pelamis device, for the whole time series. The black lines on panel (d) represent the isobaths corresponding to the optimal operating depth range of the WEC. For each selected offshore point within this range (red circles), the bivariate distributions of occurrences, corresponding to the sea states, are shown on the left side panels. Panel (a) represents the San Miguel northern point P1; (b) represents the Ensenada central point P2; and (c) Punta Banda southern point P3. On each of these panels, the wave power is represented with dashed isolines.

Comparing the efficiency of both WEC devices, Pelamis is approximately 40% more effective than Oyster2. The maximum $\bar{P}$ harvested by Pelamis is 13 kW/m, obtained inside of BTS at site P_3. In contrast, the maximum $\bar{P}$ harvested by Oyster2 is 8 kW/m and it is obtained outside the BTS, near Punta San José. Inside the bay, the maximum $\bar{P}$ harvested by Pelamis and Oyter2 are 13 kW/m in site P_3 and in site O_3, respectively.

Regarding the average values for the total time, $\bar{P}$ (proximally of 13 kW/m) occurs in the southern point O_3 (Fig. 6 (c)), whereas average values greater than 5 kW/m to 10 kW/m occur in the rest of the points. These $\bar{P}$ values correspond to H_s between 0.5 m and 1.5 m and T_e of 5 s to 17 s. In addition, of the six points analyzed, P_2 and O_1 presented the highest number of occurrences equal to 1.6% of the total incident energy with $\bar{P}$ isolines of 5 kW/m and H_s of 1 m. For P_2, T_e is 13 s, whereas for O_1 is 16 s. The maximum value for the $\bar{P}$ corresponding to one meter of wave front (of 120 kW/m) occurred in the southern section in the reference point O_3. An H_s value of about 3.7 m and T_e of 17 s corresponded to this power.

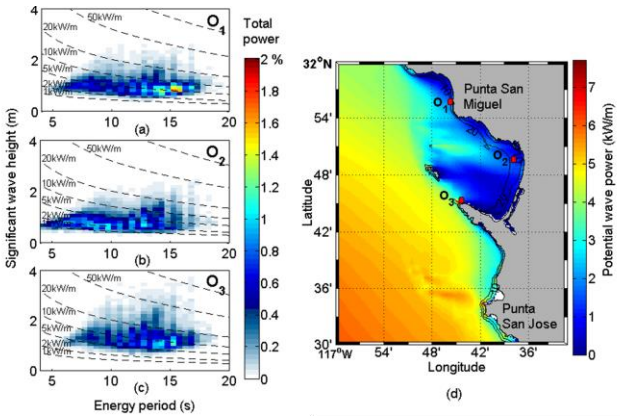

Fig. 6. Annual mean wave energy, harvested by the Oyster2 device, for the whole time series. The black lines on panel (d) represent the isobaths corresponding to the optimal operating depth range of the WEC. For each selected nearshore point within this range (red circles), the bivariate distributions of occurrences, corresponding to the sea states, are shown on the left side panels. Panel (a) represents the San Miguel northern point O_1; (b) represents the Ensenada central point O_2; and (c) Punta Banda southern point O_3. On each of these panels, the wave power is represented with dashed isolines.

H. Effect of WEC arrays on the wave field

The reduction in H_s caused by the different WEC array configurations is shown in Fig. 7. In all the cases analyzed a clear pattern can be observe, expressed by a wake of energy reduction, which extends to approximately 2500 m from the furthest first obstacle line form the coast. The greatest reduction of H_s (close to 25%) is observed just after the incident wave crosses the first obstacles. This reduction decreases as the waves propagate towards the shoreline. This is due to the dispersion of wave energy from the sides of each WEC array to the protected area downwind of the analyzed configuration [22]. As expected, the reduction of H_s increases proportionally with the number of WECs and the number of rows in the array (Fig. 7), due to the increasing absorption of energy by each row of WECs. It is also evident, that an increase in the number of rows in the array induces a reduction of wave energy and an extension of the wake area.

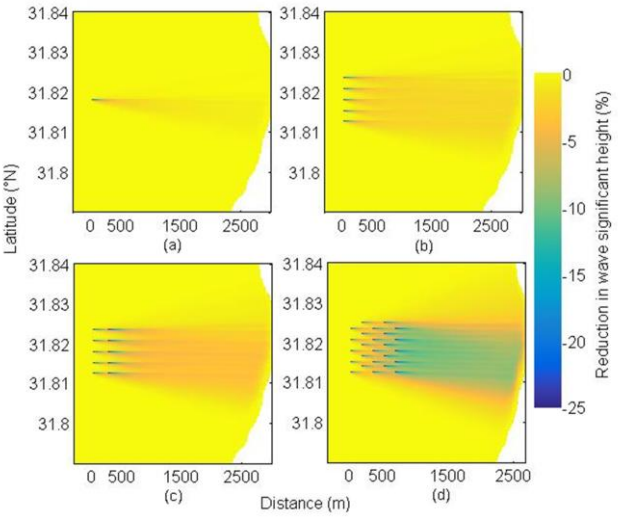

Fig. 7. Reduction in wave significant height (ΔH_s) in percentage for the various examined WEC arrays configurations: (a) single obstacle; (b) 5 vertically aligned converters; (c) 10 converters, organized in two rows of 5 devices aligned vertically and (d) staggered array, adding a total of 25 devices with the same spacing distance of devices between rows and columns.

The effect of the WECs arrays in the mean wave direction (ΔDir) is shown in Fig. 8. As it can be seen, the arrays generate ΔDir behind the array and in the surrounding area due to the angular dispersion of the dominant waves, with negative and positive variations in the lower and upper half of the devices, respectively. The greatest difference in ΔDir is observed in the wake of the staggered array (Fig. 8 (d)).

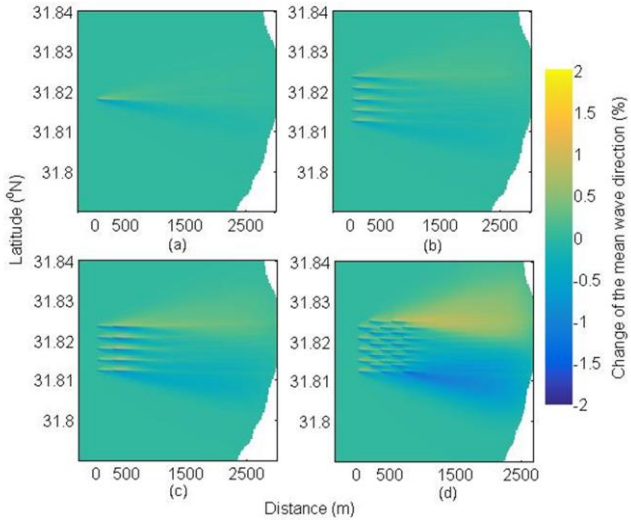

Fig. 8. Changes in mean wave direction (ΔDir) for the various examined WEC arrays configurations: (a) single obstacle; (b) 5 vertically aligned converters; (c) 10 converters, organized in two rows of 5 devices aligned vertically and (d) staggered array, adding a total of 25 devices with the same spacing distance of devices between rows and columns.

In Fig. 9 the effect of different WEC configurations on the peak period (ΔT_P) is show. As it can be seen, the WEC arrays generate changes in T_P between -2 % to 2 % with a similar pattern as described for ΔDir but, with the negative and positive variations in the upper and lower half of the devices, respectively. The positive values of ΔT_P are associated with the shift of T_P towards lower frequencies of the wave spectrum and vice versa for negative ΔT_P values. The shift of the peak in the wave spectrum could be due to the dissipation of wave energy in the peak region, redistribution of energy within the spectrum by nonlinear interactions, and wave angular spreading effects. The RCW of Oyster2 has a maximum around 0.14 Hz (see Fig. 2), thus for wave spectra with the peak at a lower frequency than 0.14 Hz, a shift of peak frequency could be expected since more dissipation (energy extraction) occurs at the peak region and higher frequencies. Nonlinear interactions usually redistribute energy from higher to lower frequencies causing a shift of peak frequency to lower frequencies however, nonlinear interactions at the leeward of the array where reduced by the presences of the WECs (not shown). Finally, since numerical experiments where forced with directional spectra, the waves at the leeward of the array come from different directions and some of them could be less affected or not affected by the WECs. This modifies the peak and mean wave direction and also could change the peak frequency of the spectrum. Also, as a consequence, the angular dispersion of directional spectra increases at the leeward of the array (not show). This effect is solely due to the differential effect of WECs on waves propagating from different directions and it is not related to wave diffraction.

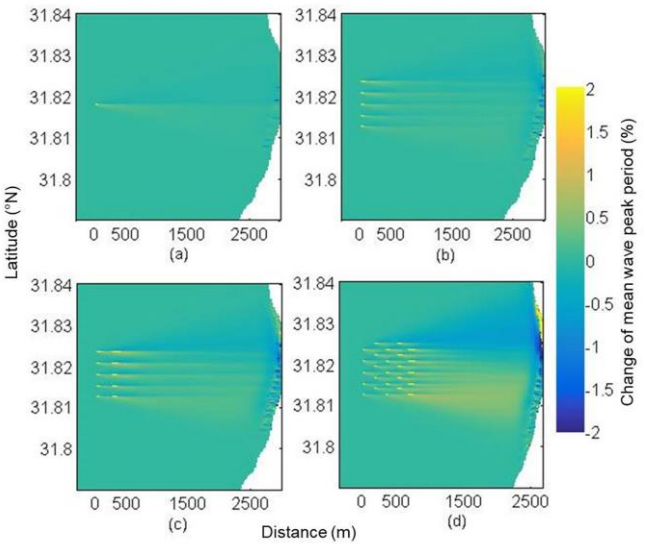

Fig. 9. Changes in mean wave peak period (ΔT_P) for the various examined WEC arrays configurations: (a) single obstacle; (b) 5 vertically aligned converters; (c) 10 converters organized in two rows of 5 devices aligned vertically and (d) staggered array adding a total of 25 devices with the same spacing distance of devices between rows and columns.

Finally, Fig. 10 shows the reduction of the wave power (ΔP) for the configuration with one WEC (Fig. 10 (b)) and the array of 25 staggered WECs (Fig. 10 (c)). As expected, ΔP has a similar behavior to ΔH_s. Most of the energy extracted by the WECs is obtained from the dominant waves, at and around the peak frequency (Fig. 10 (a)). Increasing the number of WECs or rows in the array decreases the amount of energy in the area protected by the array and makes the wake more evident (Fig. 10 (b) and Fig. 10 (c)).

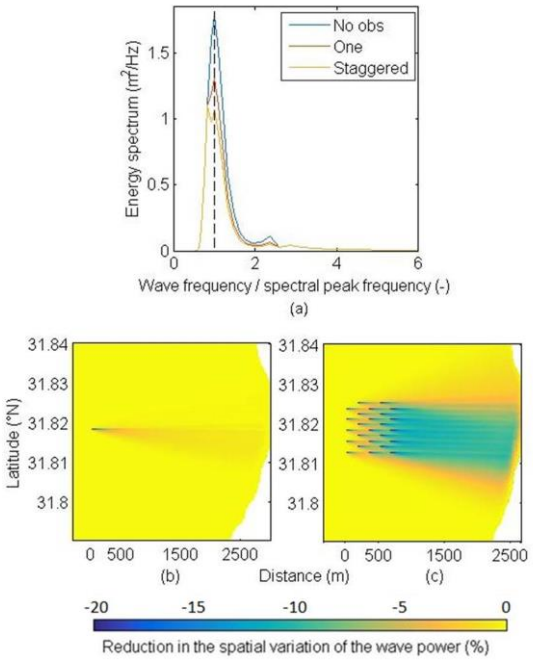

Fig. 10. Reduction in wave power (ΔP) in percentage for the various examined WEC arrays configurations: (a) associated wave energy spectrum; (b) single obstacle; (c) staggered array, adding a total of 25 devices with the same spacing distance of devices between rows and columns.

IV. CONCLUSIONS

The harvested wave energy with two different WECs within Todos Santos Bay was evaluated. The wave power availability is determined with a high-resolution wave hindcast made for the BTS and its surroundings. The hindcast spans from 2008 to 2017.

In accordance with the results, the BTS area has several sites suitable for wave energy extraction. The BTS has a moderate available wave power with a mean value around 11 kW/m. It presents a clear seasonality with higher values, around 15 kW/m, in the winter season and lower values, around 6 kW/m, in the summer. There is a large spatial variability inside BTS, caused by the sheltering effect of Todos Santos Island. In the Northern part of the BTS the wave power is almost twice that of the southern section.

The most appropriate locations for extracting wave energy were identified through the identification of wave energy hotspots and the ability of the selected WECs to extract energy of the sea states on those hotspots.

Although both devices work better in the southern region (locations O_3 and P_3) Pelamis is 40% more effective than Oyster2 on extracting the available wave power.

However, WEC configurations nearshore (depth ≤ 35 m) have bigger consequences on the environment and different social and economic activities, such as: fishing industries, maritime traffic and tourism. This is why; we focused the analysis in the Oyster2 WEC configuration that can cause a greater impact on the economic and recreational sector of the population in BTS.

The different WEC arrays configurations examined induced changes on both near-field and the nearshore wave characteristics. Its magnitude depends on the array configuration. The effect of a WEC array on the wave parameters in the nearshore increases as the number of WECs increases or the distance between the array and the shore decreases. The greatest reduction on wave characteristics was related to the wave power and the significant wave height, whereas the direction and the peak period experienced lower changes.

WEC arrays could have a significant impact on nearshore wave characteristics and the environment. Detailed studies of the effect of the array on waves, currents and sediment transport are needed for those sites susceptible of wave power extraction. A decision support tool is recommended to assist siting wave energy facilities, which allow balancing the need of profitability facilities with the need to minimize conflicts with other possible coastal uses.

ACKNOWLEDGEMENT

This work is a contribution of the CEMIE-Océano project sponsored by the fund CONACyT/SENER sustentabilidad energética (249795).

REFERENCES

[1] IEA, International Energy Agency, "World energy outlook, executive summary," 2018.

[2] H. Ritchie, M. Roser, "CO_2 and other greenhouse gas emissions," May. 2017. [Online]. Available: https://ourworldindata.org/co2-and-other-greenhouse-gas-emissions/.

[3] Diario Oficial de la Federación, "Ley de transición energética," Dec. 24, 2015.

[4] P. Gleizon, F. Campuzano, P. Carracedo, A. Martinez, J. Goggins, R. Atan, S. Nash, "Wave energy resources along the european atlantic coast," *Mar. Renew. Energy*, 2017. DOI 10.1007/978-3-319-53536-4_2, [Online].

[5] K. Gunn, C. Stock-Williams, **"**Quantifying the global wave power resource," *Renew. Energy*, vol. 44, pp. 296–304, 2012.

[6] J. Cruz, "Ocean wave energy: current status and future perspectives," Springer Series in Green Energy and Technology, Berlin, Heidelberg, Germany: Springer, 2008.

[7] R. Gonzalez-Santamaria, Q. Zou, S. Pan, "Impacts of a wave farm on waves, currents, and coastal morphology in south west England," *Est. Coast*, vol. 1, pp. 1–14, 2013.

[8] A. Ruiz de Alegria-Arzaburu, J. Vidal-Ruiz, H. García-Nava, A. Romero-Arteaga, "Seasonal morphodynamics of the subaerial and subtidal sections of an intermediate and mesotidal beach," *Geomorphology*, vol, 295, pp. 383–392, 2017.

[9] N. Booij, R. Ris, H. Holthuijsen, "A third-generation wave model for coastal regions. Part 1: model description and validation," *J. Geophys. Res.,* vol. 104, pp. 7649–7666, 1999.

[10] H. L. Tolman, "User manual and system documentation of WAVEWATCH-III Version 3.14," 2009. NOAA / NWS / NCEP / MMAB, Technical Note 276.

[11] P. Janssen, "The interaction of ocean waves and wind," Cambridge University Press, Cambridge, U.K., 2004.

[12] J. E. Stopa, K. F. Cheung, H. Tolman, A. Chawla, "Patterns and cycles in the climate forecast system reanalysis wind and wave data," *Ocean Modell.*, vol. 70, pp. 207–220, 2013.

[13] R. Henderson, "Design, simulation, and testing of a novel hydraulic power take-off system for the Pelamis wave energy converter," *Renew. Energy*, vol. 31, pp. 271–283, 2006.

[14] A. Babarit, J. Hals, M. J. Muliawan, A. Kurniawan, T. Moan, J. Krokstad, "Numerical benchmarking study of a selection of wave energy converters," *Renew. Energy*, vol. 41, pp. 44–63, 2012.

[15] C-K. Kim, J. E. Toft, M. Papenfus, G. Verutes, A. D. Guerry, M. H. Ruckelshaus, et al., "Catching the right wave: evaluating wave energy resources and potential compatibility with existing marine and coastal uses," *PloS One*, vol. 7, no. 11: e47598, 2012.

[16] D. Silva, E. Rusu, C. Guedes Soares, "Evaluation of various technologies for wave energy conversion in the portuguese nearshore," *Energies*, vol. 6, pp. 1344–1364, 2013.

[17] "Sandia National Laboratories: SNL-SWAN (Sandia National Laboratories – Simulating WAves Nearshore)," [Online]. Available at: https://energy.sandia.gov/energy/renewable-energy/water-power/market-acceleration-deployment/snl-swan-sandia-national-laboratories-simulating-waves-nearshore/.

[18] G. Chang, K. Ruehl, C. Jones, J. Roberts, C. Chartrand, "Numerical modeling of the effects of wave energy converter characteristics on nearshore wave conditions," *Renew. Energy*, vol. 89, pp. 636–648, 2016.

[19] E. Renzi, K. Doherty, A. Henry, F. Dias, "How does oyster work? the simple interpretation of oyster mathematics," *European Journal of Mechanics - B/Fluids*, vol. 47, pp. 124–131, 2014.

[20] A. O'Dea, M. C. Haller, H. T. Özkan-Haller, "The impact of wave energy converter arrays on wave-induced forcing in the surf zone," *Ocean Eng.*, vol. 161, pp. 322–336, 2018.

[21] F. Ocampo-Torres, P. Osuna, E. Rivera, I. García, T. Juárez-Díaz, "On the wave energy resource assessment in the Baja California coastal region and a study of the long term tendencies of significant wave height," in *10th European Wave and Tidal Energy Conf.*, Aalborg, Denmark, 2013.

[22] C. Beels, P. Troch, K. De Visch, J. P. Kofoed, G. De Backer, "Application of the time-dependent mild-slope equations for the simulation of wake effects in the lee of a farm of wave dragon wave energy converters," *Renew. Energy*, vol. 35, pp. 1644–1661, 2010.